RESEARCH ARTICLE

Particle & Particle Systems Characterization
www.particle-journal.com

Microfluidic Device for the Manipulation of Microparticles for Flow Cytometry Application

*Matthew Attard, David Coral, Èric Pedrol, Magdalena Aguiló, Francesc Díaz, and Xavier Mateos**

This work produces a unique microfluidic device that acts as a "lab on a chip," conducting separation, mixing, and concentration of microparticles similar to that required by cell sorting flow cytometry applications. The passive two-dimensional device shows to be successful at separating polystyrene (PS) beads between 5 and 20 µm in diameter, mixing them with an external media, and concentrating them by 250% continuously with minimal sample preparation, while still being inexpensive, and effective. By implementing the microfluidic device, the processing steps are done within seconds due to its high throughput of 2 mL min^{-1}, wherein different hydrodynamic phenomena such as Dean's forces, inertial lift forces, and enhanced diffusion are taken advantage of.

1. Introduction

HMicroparticles are present all around and inside us, but in many cases are invisible to the human eye, with a typical example being those in the blood such as platelets, white blood cells, red blood cells, and circulating tumor cells (CTCs). This being said, even though these microparticles are "invisible," they still contain information that can act as biomarkers for specific diseases such as the human immunodeficiency virus (HIV), or cancer.[1–5]

Cell debris is considered as a vector of biological information for a variety of diseases; ranging in size between 0.1 and 30 microns in diameter.[4,6,7] There are currently a variety of techniques used to detect microparticles from bodily fluid which are either defined as flow cytometry-based assays or solid phase capture assays such as enzyme-linked immunosorbent assay (ELISA), with flow cytometry preferred due to its high throughput and analysis capabilities.[6,8] Regardless, flow cytometry techniques generally require prior sample preparation before analysis takes place, as the cells to be detected generally need to be separated, mixed with an appropriate fluorescent marker, and concentrated into a smaller volume before being focused and analyzed in the flow cytometer. This being said, even though flow cytometry has high throughput and analysis capabilities, the bulkiness, cost of equipment, and duration of sample preparation are relatively substantial, therefore limiting the potential capabilities of the equipment.[6,8] This however can be alleviated by incorporating microfluidic devices in cell sorting applications; reducing the overall throughput time, size, and needed sample volume of the process.

Microfluidic devices focus on the engineered manipulation of fluids at the micron scale with one of the scopes being the detection, analysis, and/or manipulation of different micro-, and nanoparticles within a fluid or gas.[5,9–11] This provides solutions for applications in both chemical and biological fields.[5,9–14] This variety stems from the designers' ability to implement a diversity of component designs into one microfluidic device, where each component is responsible for a single function. Therefore, a well-constructed microfluidic device made of multiple functional components can be considered a "lab on a chip," where previously lengthy processes and large, complex equipment is miniaturized into a simple, portable device of a small volume (few cm^3). These advantages are attributed to the size of the microchannels within the device, where low Reynold numbers (ratio between inertial and viscous forces) prevail, and forces such as Dean's and inertial lift forces are taken advantage of to allow for the parallelization of different processes.[15]

Currently, when we consider microfluidic devices for flow cytometry applications, a large amount of focus is placed solely on improving individual component designs for specific applications rather than creating a complete lab on a chip. Such can be seen in a variety of works such as that of Pedrol et al.,[16,17] who focused on rare CTCs for the early detection of breast cancer using a three-dimensional, passive microfluidic device that confined, and quantified the amount of HER2 cells from a sample,

M. Attard, D. Coral, M. Aguiló, F. Díaz, X. Mateos
Universitat Rovira i Virgili
URV
Física i Cristal·lografia de Materials
FiCMA Marcel·lí Domingo 1, Tarragona 43007, Spain
E-mail: xavier.mateos@urv.cat
È. Pedrol
SRCiT – Service for Scientific and Technical Resources Campus Sescelades N2 building
Universitat Rovira i Virgili
Països Catalans 26, Tarragona Av. 43007, Spain

The ORCID identification number(s) for the author(s) of this article can be found under https://doi.org/10.1002/ppsc.202300038

DOI: 10.1002/ppsc.202300038

similar to what is done in cell sorting flow cytometry techniques but in a much smaller, simpler, and cheaper device. Alternatively, Hou et al.[3] obtained CTCs directly from the blood by incorporating a two-dimensional, passive device for their separation from leukocytes and red blood cells due to their variation in diameter, of approximately 15–20, 7–12, and 6–8 μm, respectively. After said separation, the CTCs are then utilized on varying capture assays for disease diagnosis. On the other hand, other efficiently catered passive two-dimensional designs are illustrated in the works of Carlo et al.,[18,19] and Zheng et al.,[20] who developed highly efficient, simple designs to respectively separate and mix different microparticles, polystyrene (PS) beads, and *E. coli*, among others by taking advantage of Dean's forces, inertial migration, and diffusion within fluids. These are only a few examples where individual components of the flow cytometry process are utilized independently for a specific task. If on the other hand such components were linked together, it could facilitate sample preparation for cell sorting in flow cytometry.

For this reason, we are seeking to create a simple microfluidic device that can run continuously while consisting of two-dimensional, passive components being a separator, mixers, and concentrators. All of these shall be studied using PS beads ranging between 5 and 20 microns in diameter, therefore mimicking a variety of natural cells within the body, such as blood cells, leukocytes, T-lymphocytes, and CTCs among others as proven by previous authors.[3,16–20]

A large variety of processes within a passive microfluidic device are utilized by taking advantage of different forces and fluid dynamics where the size of the device's microchannels allows for laminar flow, meaning low Reynolds numbers. This adversely prevents chaotic flow within liquids, allowing for a controlled stream that can be manipulated through linear diffusion, Dean drag or inertial forces. These forces show to be effective in a variety of designs such as micro-separators, mixers, and concentrators among others.

Separators are utilized for the separation of particles by size to be used for detection purposes or easier analysis. A particular separator of interest was produced by Bhagat et al.[21,22] who developed a simple design, wherein Dean coupled inertial migration and inertial lift forces separates microparticles along specific bands within the microchannels and found that microparticles between 1.9 and 20 μm can be separated with separation efficiency of approximately 90%. This was proven with PS beads of varying sizes and with organic matter; C6 glioma cells and SH-SY5Y neuroblastoma cells. Alternatively, Martel et al.[23] extended the design proposed by Carlo et al.[18,19] by adding a well-placed siphoning channel adjacent to the separating/confining channel, where microparticles/cells are separated due to the Dean and inertial lift forces present, allowing for concentrations exceeding 50× the original concentration.

The total inertial lift forces (F_L) within the channels act on the particles from the combination of wall-induced lift forces, and shear-induced lift forces[24] Due to Poiseuille's flow, the microparticles flowing along the microchannels incur shear-induced lift forces causing it to move toward the walls until a point wherein the wall-induced inertial lift forces are predominant.[18,22] For this reason, microparticles occupy specific equilibrium positions along narrow bands of the microchannel due to the opposing lift forces.[25,26] Since varying microparticle sizes elicit a different ratio of wall and shear induced lift forces, the equilibrium position along the channel varies, therefore allowing for efficient separation.[25,26] From the lift forces alone, the microparticles will focus along a band at each of the four walls in the microchannel, but since Dean's flow is present due to centrifugal forces, this is reduced to one narrow band which forms along a single zone between the inner or outer wall of the microchannel.[21,22]

The Dean drag forces are present when instabilities are present laterally along the cross-section. This is a characteristic of Dean flow, and magnitude of such forces is dependent on the dimensionless number, better known as the Dean number (De) which directly relates to the Reynold's number (*Re*), given by:

$$De = \frac{p U_f D_h}{\mu} \sqrt{\frac{D_h}{2R}} = Re\sqrt{\frac{D_h}{2R}} \tag{1}$$

where p is the density of the fluid (kg m^{-3}), U_f is the average velocity of the fluid (m s^{-1}), μ is the fluid viscosity (kg m^{-1} s^{-1}), and R is the radius of the curvature of the channel path (m). For separation and confinement, a low Dean numbers will prevent recirculation and therefore allow for easier isolation of microparticles of varying sizes.[18,24,27]

The dean vortices along the microchannel exert a drag force on microparticles depending on their size according to stokes drag equation[24,28] given by:

$$F_D = 3\pi\mu U_{Dean}\, a_p = 5.4\times10^{-4}\,\pi\mu \mathrm{De}^{1.63} a_p \ (N) \tag{2}$$

Since according to Ookawara et al.[28] the average Dean velocity is given by:

$$U_{Dean} = 1.8\times10^{-4} De^{1.63} \ (\mathrm{ms}^{-1}) \tag{3}$$

This force is responsible for how the particle flows along the microchannel, while the lift forces (shear and wall-based) account for the lateral migration of the microparticles. This lift force can be quantified by the equation derived by Asmolov,[24] given by:

$$F_L = pG^2 C_L a_p^4 \ (N) \tag{4}$$

where C_L is the coefficient of lift as a function of the position of the particle along the microchannel cross-section. G is the average fluid shear rate (s^{-1}). From Equations (2) and (4) respectively, we can derive that the Dean and lift forces directly relate to the size of the particle such that $F_L \propto a_p^4$ and $F_D \propto a_p$, by adjusting the ratio of these forces, different migrations are obtained based on particle size.[21,22] A separator and concentrator may therefore be optimized depending on microparticle sizes, microchannel dimensions, and the fluid velocity along the microchannel.

Mixing on the other hand is mainly based on the diffusion of adjacent liquids. In the macroscale, high Reynold's numbers are prevalent, making mixing relatively easy due to the random eddies that fold and stretch the fluid chaotically.[29] If no turbulence is present, diffusion will take longer due to the distance that the liquid must diffuse before being mixed. This can be considered to be the case for laminar flow in microfluidic devices due to a small Reynold's number preventing the formation of natural eddies or currents.[30] Long microchannel lengths are therefore required for efficient mixing in laminar-based patterns. The

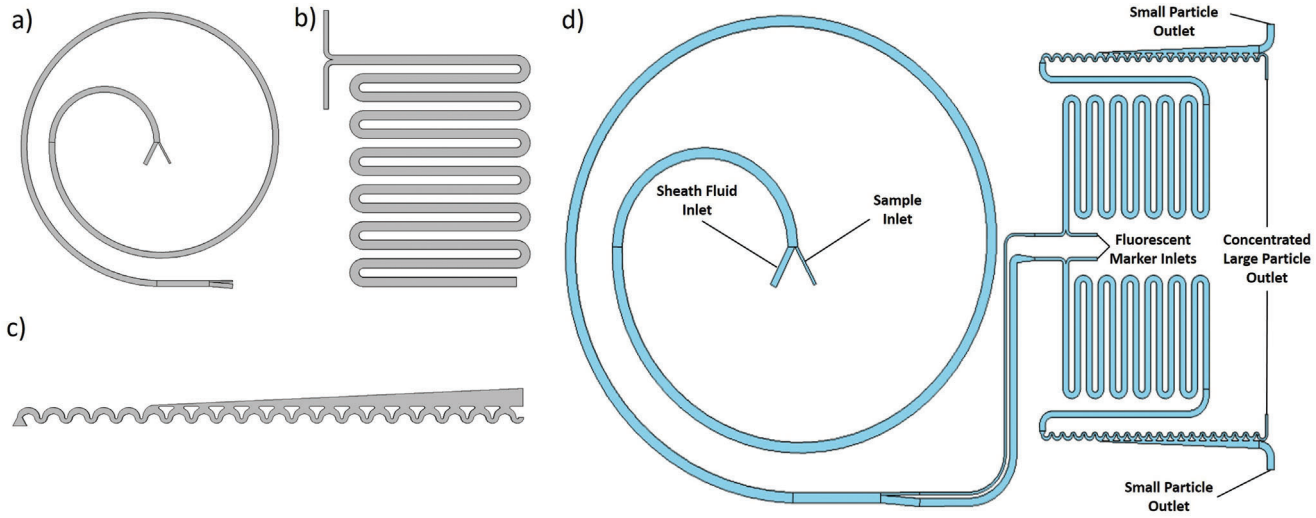

Figure 1. Illustrations consisting of the a) separator, b) mixer, c) confiner, and d) the final microfluidic device design developed.

earliest of which is realized through the works of Kamholz et al.[31,32] with the T-type and Y-type mixers, which consist of two inlet fluids which combine along a straight channel solely through diffusion. Diffusion relies on the dimensionless number known as the Péclet number (Pe) which linearly determines the mixing efficiency calculated by using:

$$\mathrm{Pe} = \frac{U_o w}{D}$$

where U_o is the fluid velocity (m s^{-1}), w is the channel width (m), and D is the diffusion rate (m^2 s^{-1}). By utilizing this equation, we can determine the distance required for mixing by diffusion to occur in a T- or Y-type mixer. The simplicity of the two-dimensional design makes it easy for fabrication and testing purposes but due to the high area footprint, the designs have been modified by a variety of authors[20,33–37]

2. Experimental Section

The scope of this study is to create a lab on a chip that acts as a miniaturized system synonymous with the preprocessing required for flow cytometry applications, while retaining throughput and microparticle viability. The device will consist of two-dimensional, passive components that will function according to a variety of hydrodynamic concepts that govern microfluidics.

To achieve this goal, the proposed device will consist of multiple components, being, a separator, mixers, and concentrators. The separator as illustrated in **Figure 1**a will separate PS beads with a diameter of 20 µm from those of 10 and 5 µm by taking advantage of inertial lift and Deans forces. The importance of a separation process is clear in the work of Hou et al.[3] who found that CTCs within the bloodstream are very minute ranging between 5 and 88 CTCs per mL of blood for patients with stage III cancer or above. This being said, the separation of rare CTCs from the blood makes them easier to be detected and processed, especially since all other constituents in the bloodstream, such as blood cells (approximately 10^9 blood cells per 1–100 CTCs) are removed.

The separator is connected to two mixers (one for each outlet) that have a simple design as illustrated in Figure 1b,d. This is incorporated since the size distributions of CTCs and normal cells may overlap, with previous separators showing 90% separation,[21,22] whereas a second discrimination method (labeling) is applied to pinpoint the presence of CTCs. In this design, fluid is mixed by diffusion as governed by the Pe as well as enhanced advection of the fluid caused due to the forces created at the curvatures. This design will therefore allow for the effective mixing of fluid quickly due to a few factors. Firstly, shorter distances of diffusion are needed due to the small cross-sectional dimensions of microchannels. Secondly, due to the presence of enhanced advection, mixing is further improved due to the reduced distance created between the liquids. Finally, due to the total length and reduced cross-sectional dimensions of the microchannel, the microparticles have a higher likelihood of reacting with their constituent fluorescent markers since they are in contact with them for a longer time.

A concentrator will then be connected to the mixer outlets, with the design modified from the works of Martel et al.[23] and Carlo et al.[18,19] as illustrated in Figure 1c,d. In this design, the concentrator allows for the microparticles to be focused along a specific streamline, confined within the microchannel depending on the microparticle size as described by Carlo et al.[18,19] The microparticles will then continue flowing in such a manner while the liquid is siphoned out from the adjacent channel, inadvertently increasing the concentration of microparticles while also reducing the velocity of the main channel. Moreover, since microparticles of varying sizes are flowing in curved channels, Deans, and inertial lift forces, push larger particles closer toward the inner walls. This means that smaller particles will be closer to the outer wall, allowing for them to be siphoned out if necessary. This concentrator therefore cannot only concentrate particles but also focus them and siphon out smaller ones, which is an unnecessary yet positive add-on to the device.

All these designs, besides being tested individually have also been combined to create the proposed device as illustrated in Figure 1d. The components were initially studied using simulations. From this, an experimental study was conducted where the components and final device were fabricated and tested to compare experimental and simulation-based results.

2.1. Computational Modeling

Computational modeling was conducted using Comsol Multiphysics v5.4 to visualize the two-dimensional velocity and pressure fields as well as the three-dimensional particle trajectories for specific geometries.

The component geometries were created using the inbuilt Comsol platform, and Clewin4 wherein the height of the microchannels for all components was kept constant at a value of approximately 155 μm while other channel dimensions (width, lengths, curvatures etc.) were varied accordingly for each design. By doing so, creating a two-dimensional design wherein each component forms complementarity toward one another. Once the geometries were established, the physics was then defined in the platform. Due to the size of the channels, the Navier-stokes equations were solved for laminar flow conditions. The simulation conditions were restricted to incompressible flow and no-slip boundary conditions against the walls.

The normal inflow velocities were initially calculated solely for the separator according to the equations described earlier, accounting for the required Dean and inertial lift forces to separate the microparticles. However, the mixer's inlet velocities were determined from the resulting outlet velocity of their adjacent connecting channels of the separator. The same can then be said for the concentrator, where the inlet velocity was obtained from its adjacent connecting channel, being the outlet of the respective mixer. The mesh for each component was then set to a physics-controlled "coarser" mesh before computing. Laminar flow was computed as a stationary study, resulting in two-dimensional plots of the pressure, and velocity fields within the microchannels, as well as other two- or one-dimensional complimentary results, as required.

The particle trajectory study was conducted for PS beads of diameters 20, 10, and 5 μm diameters while considering Newtonian formulation. The inlet velocity is directly dependent on the previous study (laminar flow) where the particles flow along the channel according to the velocity and pressure profiles. The particles were released from the inlets based on the coarseness of the mesh and interacted with the walls, such that they would bounce off them depending on their initial momentum. This aside, Drag forces and inertial lift forces were implemented along all the component designs to simulate the relevant forces on the particles. Once these parameters were set, a time-dependent study was computed, resulting in three-dimensional plots of the particle trajectory within the microchannels.

This methodology was implemented for each component. This however was not repeated for the final design as the components' cross-sections and velocities are analogous to one another, therefore once the components are attached, it is expected to function the same way as in the individual component simulations. Furthermore, the mixer also went through an additional study step that consisted of the transport of diluted species, which is a simple stationary study illustrating how two fluids of different inlet concentrations will react toward one another within the microchannels.

2.2. Experimental Procedure

The experimental procedure was carried out for four designs, a separator, mixer, concentrator and the full design, all of which are illustrated in Figure 1. This was decided with the aim of not only confirming the results obtained in simulations but also proving the functionality of the final device.

A standard photolithography fabrication method was used to fabricate our devices as illustrated in **Figure 2**, Due to the required thickness of approximately 155 μm, a highly viscous photoresist was chosen, SU8-2150 (MicroChem Corp., Newton, MA, USA). The master molds containing the channel geometries were used repetitively in the soft lithography procedure to fabricate the final device as illustrated in Figures 1 and 2. The microchannels were then cleaned by passing detergent diluted at a ratio of 1:100 with DI water at relatively high speeds using a syringe, followed by a subsequent cleaning with water.

After fabrication, the device components and final design were tested by passing green monodispersed fluorescent PS beads with diameters of 5, 10, and 20 μm (microparticles GmbH, Berlin, Germany) within the microchannels. The microparticles were prepared by diluting them in DI water to a concentration of 0.125% weight by volume. The device then had tubes of 500 μm diameter inserted in the inlets and outlets. The outlets tube ends were placed into a waste container with no pressure applied, while the inlets were connected to a pressure controller (OB1-mk3 from Elveflow, Paris, France) allowing for the application of pressures ranging between 0 and 2000 mbar at each inlet.

A single laser diode (06-01 Series from Cobolt AB, Solna, Sweden) coupled to an FC/PC optical fiber coupler was mated to a 1×2 single mode fiber splitter at a ratio of 50% transmitting a light wavelength of 473 nm (FC488-50B-APC-1 from Thorlabs Inc., Newton, NJ, USA). This wavelength was guided to the desired areas that were being studied while microparticles were flowing in the microchannels. The 473 nm wavelength produced is pumped through the coupled optical fiber with a current of 120 mA, allowing for the microparticles to fluoresce, making them visible when using an inverted microscope (IN480TC-FL from AMScope Inc., Irvine, CA, USA). Once a laminar flow is maintained, the microscope is used to obtain static images or videos, which are utilized for further analysis of the microparticle trajectory within the devices for different pressures and particle diameters.

This process was repeated for all the component designs and the final device, with results cross-checked with the relevant simulations. Furthermore, besides microparticle flow analysis, diffusion was also studied in the mixer component by incorporating a blue organic dye of high concentration and passing it through the channel alongside a stream of DI water and/or microparticles.

3. Results and Discussion

Within this section, four microfluidic devices have been fabricated to study how microparticles are manipulated within the

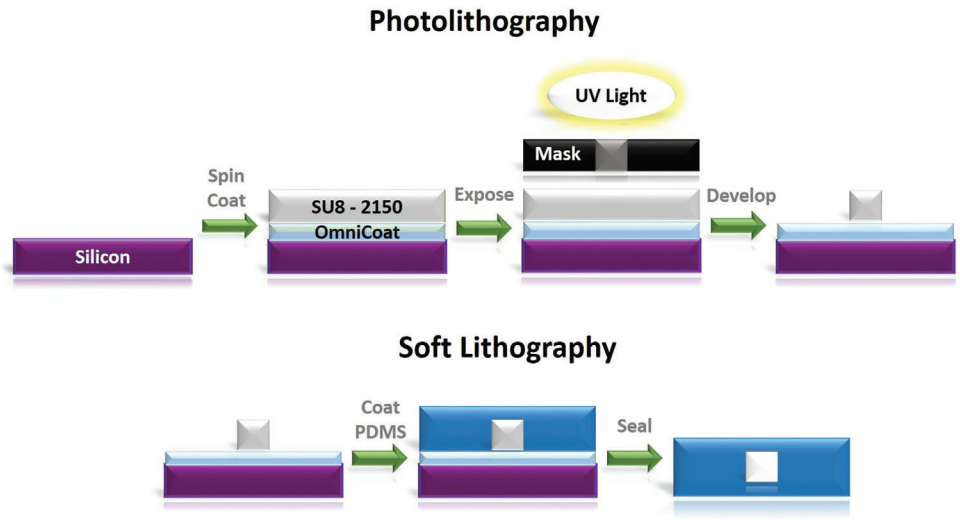

Figure 2. Simplified illustration of the photolithography and soft lithography process utilized.

different geometries proposed. These four device geometries include a separator, mixer, confiner and the final device, as illustrated in Figures 1 and **3**, and have been fabricated and studied by using the previously mentioned methodology.

3.1. Fabricated Components

For our application, a thickness of approximately 155 μm was required, and after adjusting the spin speeds accordingly, it was found that the appropriate speed is approximately 2250 rpm when 3 mL of SU8-2150 was deposited on the surface of the 3-inch silicon wafer. The final thicknesses obtained for the separator, mixer, confiner, and final device are 155.2 ± 3.1, 147.5 ± 3.0, 153.2 ± 3.6, and 154.2 ± 5.2 μm, respectively, meeting our requirements. However, there is a rather large variation in thickness along each design, that occurs due to the high viscosity of the SU8-2150, wherein any defect present on the silicon substrate and/or photoresist, such as air bubbles, scratches, dirt, etc., causes an uneven distribution of the resist. Nevertheless, this thickness variation should not drastically vary the results obtained from any of the designs, as the particle trajectories and diffusion are rather dependent on the component design rather than the thickness.

Figure 3. Final device fabricated, consisting of a separator connected to mixers and concentrators.

The dimensions on the surface have very high precision, made possible by the masks manufactured using the UV lithography laser, wherein the dimensions are precise down to the submicron level. This, alongside the tight seal created between the mask and the SU8-2150 surface during exposure allowed for accurate dimensions with a deviation from the actual value of approximately ±0.6%.

The above information has therefore outlined that the dimensional accuracy for the surface features is rather high, while the thickness of the channels has some slight variance. This is believed to be satisfactory for our applications.

3.2. Component: Separator

The separator proposed is aimed at separating 20 μm diameter PS beads from others of 10 and 5 μm in diameter, by taking advantage of Dean's and inertial lift forces. This was accomplished through the design illustrated in **Figure 4**a through simulations and experimental analysis.

Through simulations, the importance of these forces became clear as the flow rates were varied, consecutively varying these forces according to Equations (2) and (4). This concurrently meant that particle separation within the design will only occur at a given flow rate, having a specific De. This can be seen when taking three different flow rates and therefore three De illustrated in Figure 4b–d. From the simulations we derived that at a low dean number, not enough time is allowed for the particles to migrate toward the outer wall and therefore separate, meaning that the forces acting on the particles are too low. On the other hand, if the forces are too great, recirculation of the particle streams will occur, consistent with the findings of Bhagat et al.[22] No separation for these flow rates therefore occurs as a full dean cycle has not been maintained within the design. A full dean cycle is formed when a particle of a given diameter migrates from the

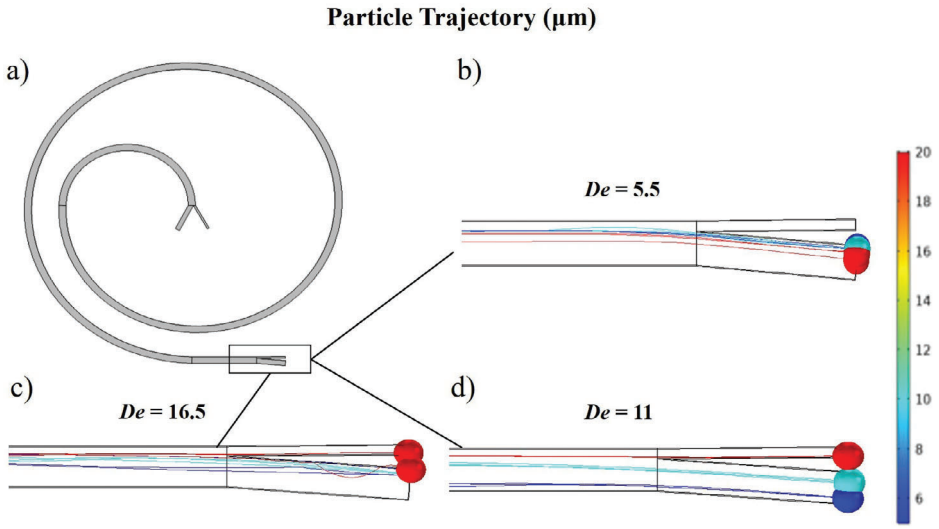

Figure 4. a) Illustration of the separator design. Particle trajectories at the outlet of the separator of PS beads flowing under varying flow rates with Dean numbers of b) 5.5, c) 16.5 (all beads are overlapped in the lower channel), and d) 11.

initial position at the inner wall within the microchannel toward the outer wall. The Dean cycle varies for each microparticle because of their size due to the forces present and longer or shorter channels may be needed if a full Dean cycle isn't maintained for a given De. However, a balance can be found by implementing Equations (1)–(4), to find the adequate flow rates for efficient particle separation as illustrated in Figure 4d.

Following these results, we commenced toward experimental analysis where the pressures were adjusted to produce the required forces while also forcing the microparticles at the inlet toward the outer wall as illustrated in **Figure 5**a. Similarly to simulations, when too low a flow rate was applied, the microparticles could not be separated. However, as the flow rate increased, the required Dean cycle was maintained, therefore allowing for microparticle separation, where the PS beads form isolated distinctive streams depending on the microparticle diameters as illustrated in Figure 5b–d following pathways nearly identical to that of simulations in Figure 5d. The design therefore has the

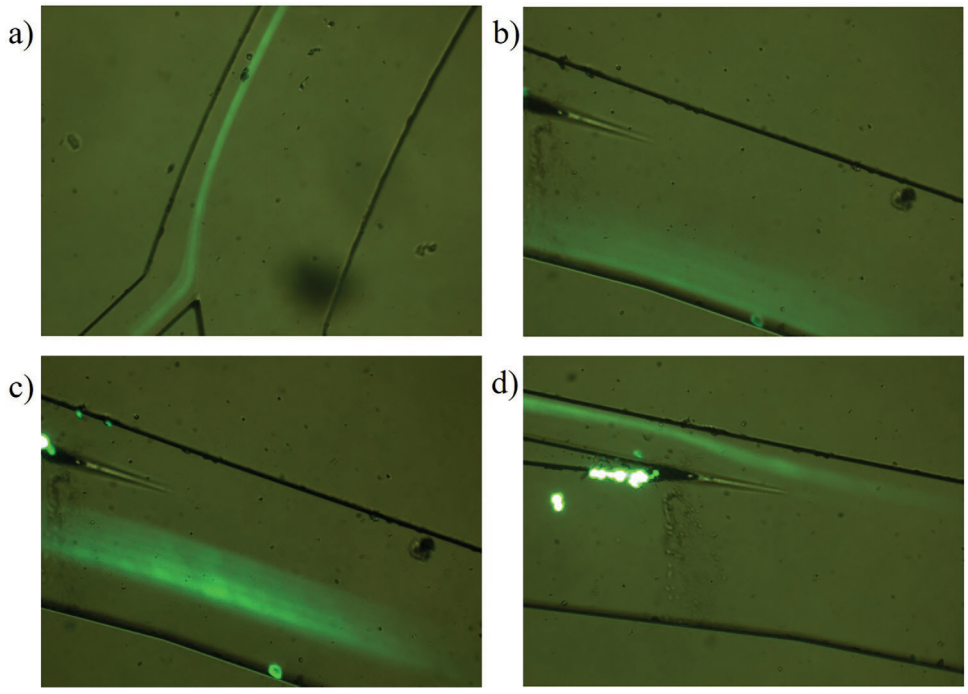

Figure 5. Microfluidic device sections showing how microparticles flow along the a) inlet and, b–d) the outlet for PS bead diameters of b) 5 µm, c) 10 µm, and d) 20 µm at the required flow rate.

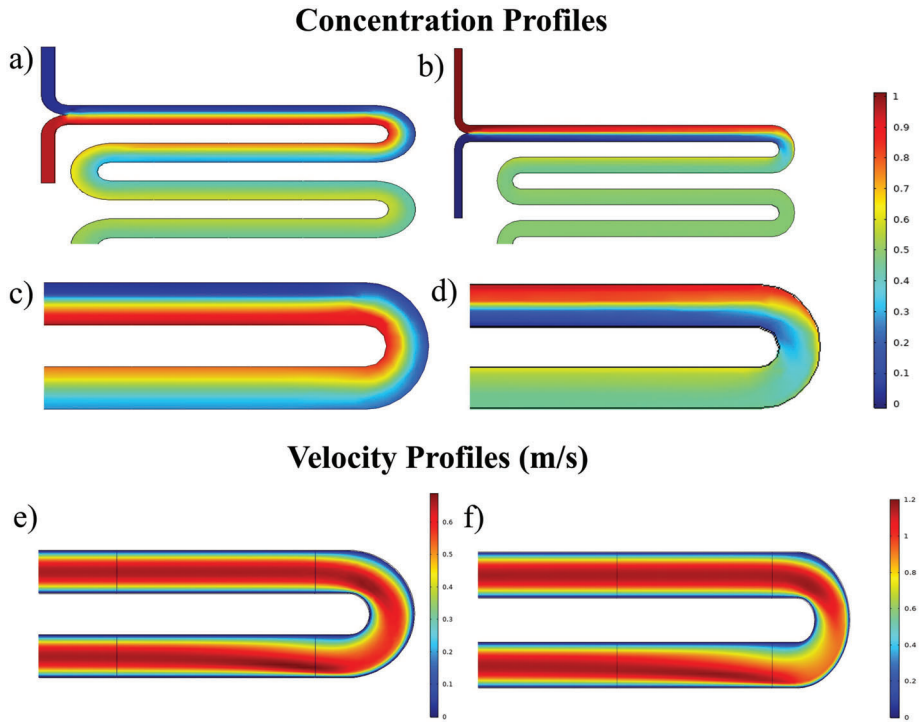

Figure 6. Simulations showing how two liquids of different concentrations mix at an inlet pressure of a) 50 mbar and b) 400 mbar. Velocity profiles for inlet pressures of c) 50 mbar and d) 400 mbar and a focused view of how the fluids interact at the first-row curvature at inlet pressures of e) 50 mbar and f) 400 mbar.

capability of separating these three microparticles into three distinct streams allowing for the 20 μm PS beads to be separated from the other beads at an efficiency exceeding 95% as seen in other research work conducted by other authors.[21,23]

3.3. Component: Mixer

The mixer proposed has a rather simple design with the aim of mixing fluids such as dyes and fluorescent biomarkers with the adjacent microparticles. In our case, the modified T-mixer design illustrated in Figure 1b was chosen. In this design, two areas are involved in the mixing procedure, the straight and curved channels, in the former, mixing occurs solely through diffusion according to the Pe described by Equation (5). On the other hand, as the straight channel meets the curvature, mixing is enhanced, as the direction of the fluids and their constituents are varied abruptly, in turn causing improved mixing due to the circulation of the fluid.

With this in mind, we first designed our mixer based on simulations wherein mixing would mainly occur through diffusion and/or circulation. We found that for both cases, full mixing occurs rapidly for a fluid consistent with a conservative diffusion rate of 1×10^{-11} m^2 s^{-1} as illustrated in **Figure 6**a,b, respectively. However, it can be seen that at low flow rates with inlet pressures of 50 mbar, no recirculation occurs at the curvatures, as the fluid's direction is not abruptly varied, since the velocity variations along the curvature are not large enough as illustrated in Figure 6e. However, when the velocity is increased, distinctive velocity variations are present as illustrated in Figure 6f, meaning that circulation is more likely to occur, enhancing the mixer's efficiency as illustrated in Figure 6c,d.

These results were then directly confirmed in the experimental analysis as illustrated in **Figure 7** where we can see that near-to-full mixing occurs at all pressures as illustrated in Figure 7c. We then commenced studying how the mixer operates at higher flow rates, taking advantage of the curvatures to efficiently mix the fluid. We can visualize these phenomena in Figure 7a,b where we can see how increasing the flow rate will determine which is the predominant mode of mixing, whether through diffusion or by these chaotic events. Initially, at 60 mbar we can see that due to the low flow rates no chaotic events occur therefore mixing occurs solely based on diffusion. However, as the flow rate increases, so does the mixing efficiency, which can be seen immediately after the initial curvature where mixing is substantially enhanced. This however occurs between inlet pressures of 200–500 mbar, after which, the high flow rates tend to cause the fluids at the curvatures to recirculate to the point that the position of the dye starts to shift toward the upper wall rather than the lower wall as expected. This change is initially rather small as the flow rate exceeds the optimum level of 400 mbar, but at a flow rate of 1000 mbar it becomes rather evident as the rows' concentration profiles are seemingly identical, making the design again rely solely on diffusion as illustrated in Figure 7.

This procedure was then repeated for microparticles of 20 μm in diameter, with the pressures varied accordingly, and it can be seen that the microparticles are in contact with the dye after surpassing the first curvature for all flow rates as illustrated in Figure 7d. The microparticles should therefore have the capability of reacting with the respective dye or marker given that

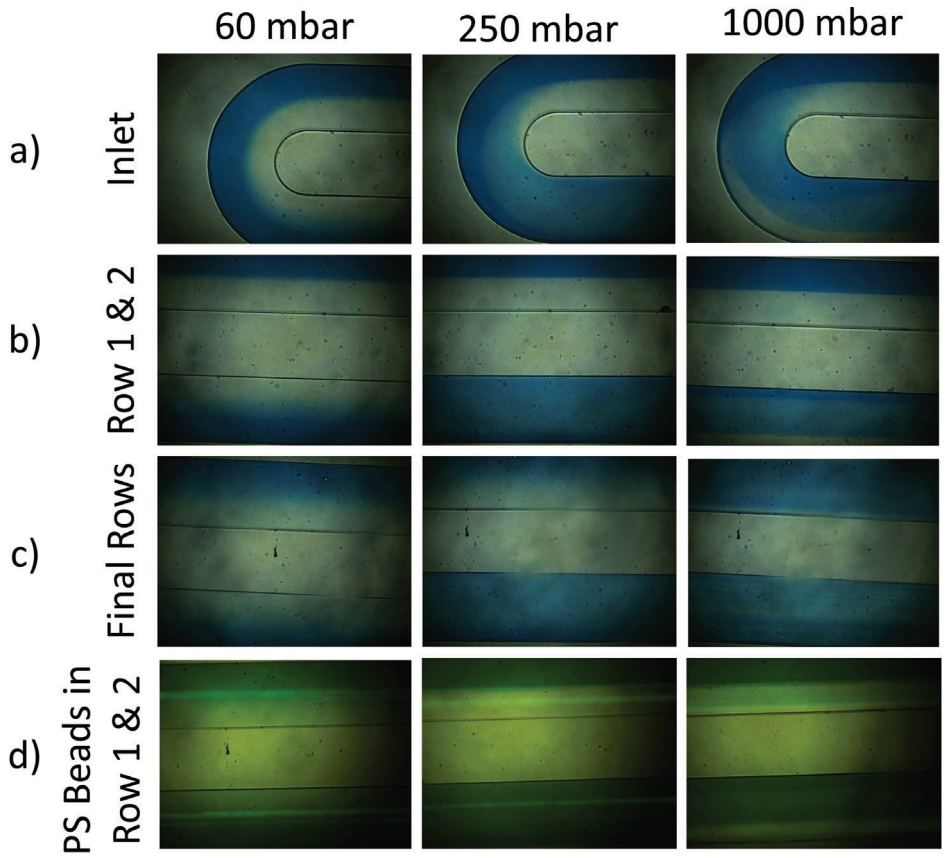

Figure 7. Experimental analysis of the mixer for pressures of 60, 250, and 1000 mbar at a) the inlet, b) the first two rows, c) the final two rows, and d) the first two rows with fluorescent microparticles.

they are in constant contact with one another for an elongated duration.

3.4. Component: Concentrator

The concentrator chosen as illustrated in **Figure 8**b consists of a channel that focuses microparticles in individual streams and is then concentrated or siphoned out depending on the PS bead diameter. This was proven through simulations as illustrated in Figure 8c,d where it is seen how the 20 μm diameter particles are focused and concentrated along the inner walls of the channel. It can then be seen that within the siphoning area, their velocity is reduced as illustrated in Figure 8a, concurrently increasing the concentration of microparticles as they progress toward the outlet. On the other hand, the 5 μm particles are too small and focus themselves away from the inner wall making them vulnerable to be siphoned out of the main channel, which in fact occurs at the siphoning area as illustrated in Figure 8c. Similarly, can then be seen for the 10 μm diameter particles that are only partially siphoned from the main channel as the focused stream is at a position that barely exceeds the siphoning limit. Through simulations we therefore found that our design has the capabilities of concentrating, separating, and focusing microparticles along a microchannel but this may vary for the experimental analysis as the designs dimensions and experimental conditions must be optimal for this to occur.

Given the results found through simulation-based analysis, we commenced with an experimental study using the same design. The design was initially run with 20 μm sized PS beads wherein we realized that focusing did not occur along a single stream within the microchannels but formed one or two distinctive streams along the inner and/or outer walls as illustrated in **Figure 9**a. Similarly was found in the works of Carlo et al.[19] where this designs geometry and De was varied until a single stream was produced. After, the streams then went into the siphoning section wherein the stream forming along the outer wall was siphoned out, while that along the inner wall remained within the main concentrating channel as illustrated in Figure 9b,c. The microparticles within the main concentrating channel then traverse at a slower rate when compared to those at the siphoning channel allowing their concentration to respectively increase as expected. This was then repeated for PS beads with diameters of 10 and 5 μm and it was found that similar results were present for the 10 μm sized PS beads when the same conditions were maintained.

However, the PS beads were focused closer toward the outer wall due to the forces acting on them, making them more susceptible to siphoning. The particles can therefore only be partially concentrated as illustrated in Figure 9d. On the other hand, when this was repeated for 5 μm sized PS beads, none of this occurred

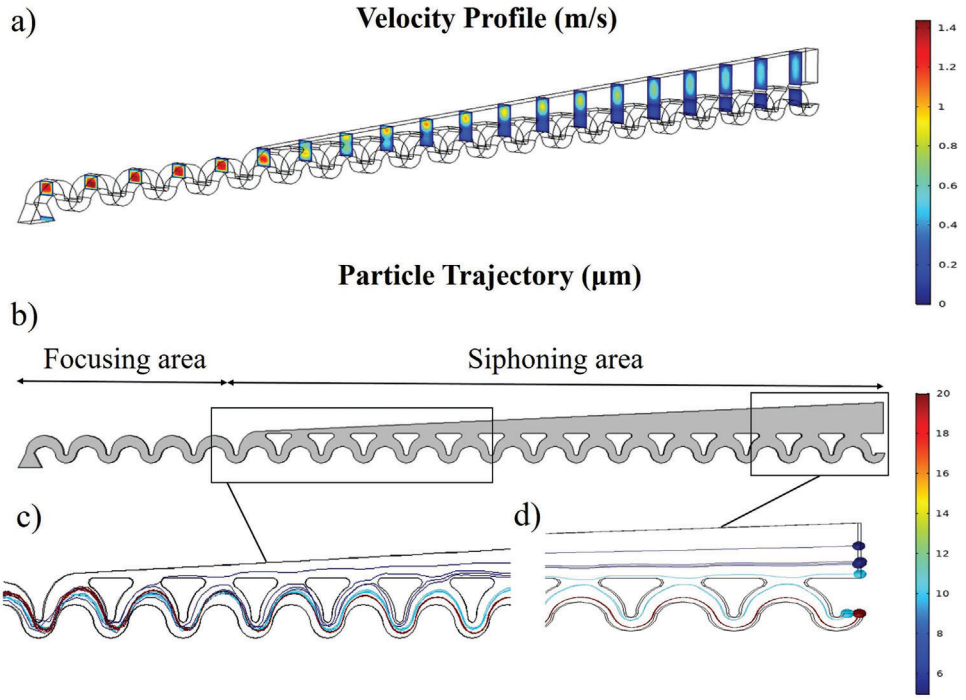

Figure 8. a) Simulation showing the velocity profile along the length of the concentrator regardless of particle diameter, where velocities in the siphoning channel are higher than of the main focusing channel. b) The geometry of the concentrator design microparticles of varying sizes are focused, concentrated, and separated as seen in the c) beginning and d) end of the siphoning area.

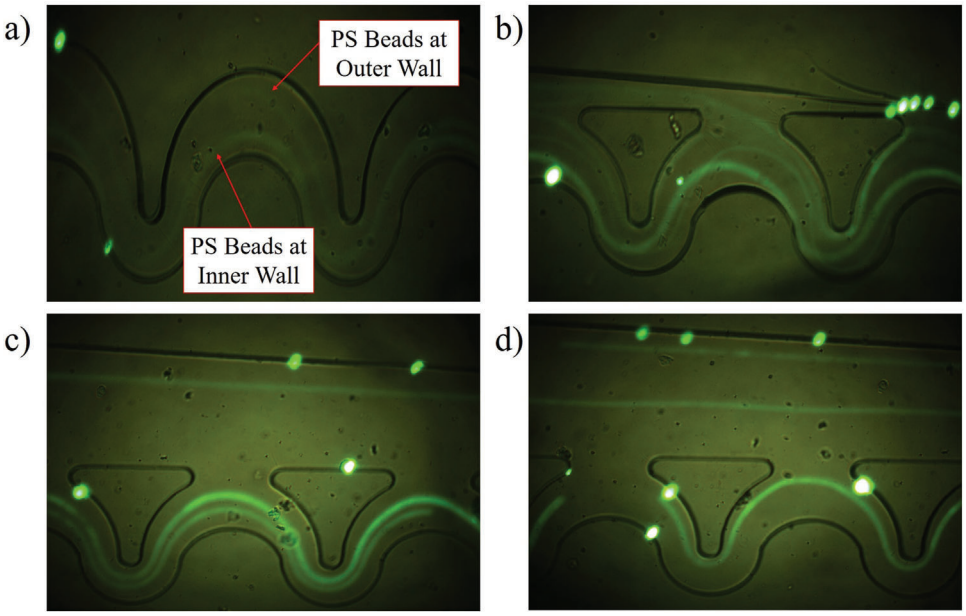

Figure 9. Concentrator proving how a) 20 µm particles focus into two distinctive streams along the walls, b) how the particles at the outer wall are siphoned out, c) how the microparticles along the inner wall are concentrated in the main channel. d) The outlet area of the concentrator shows how 10 µm particles are concentrated along the outer wall of the main channel.

as the beads were not focused within the main channel but instead flowed regularly under laminar flow conditions. This is believed to be the case as low inertial lift and dean forces acted on them in turn meaning that no siphoning or concentration of the particles occurred, contrary to the findings of Martel et al.[23]

This aside, the concentrator has the capability of focusing microparticles down to a concentration of approximately 250% of the original value as found by repeatedly running liquid through the inlet and measuring the outlet masses using a precision scale. This, as well as the information previously outlined means that

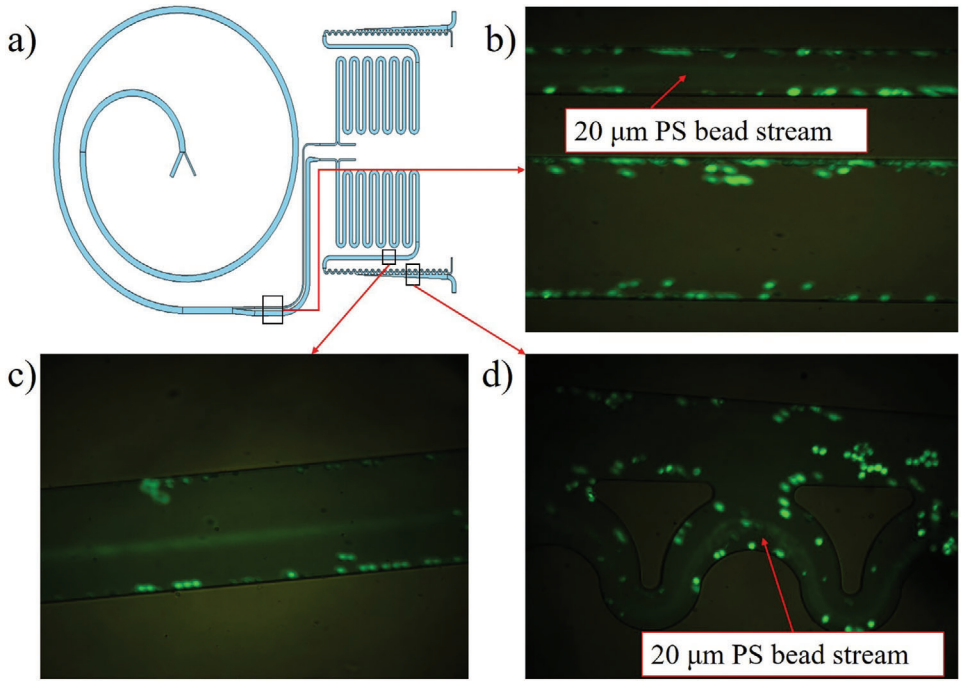

Figure 10. a) Illustration of the final design. A total of 20 um beads being continuously and simultaneously, b) separated to the required channel, c) mixed with a dye, and d) concentrated.

the concentrator has been proven to be somewhat effective for the 20 μm sized PS beads as required, while still being partially effective for 10 μm sized PS beads, therefore somewhat mimicking the simulations made. This being said, there is the possibility of reusing the lost material at the siphoning outlet by passing it through the device again. This is considered to be rather viable as the process occurs rapidly, taking up only a fraction of a second. However, if this were to occur, the concentration will inevitably be slightly reduced, while retaining time efficiency and increased microparticle retention.

3.5. Final Device

The final device as illustrated in **Figure 10**a contains all three components described earlier. Given their functionality, they are expected to function when combined with the device being tested using only 20 μm PS beads.

The initial conditions for the separator were maintained according to the effective pressures found earlier in section 3.2, proving that separation still effectively occurs as illustrated from the outlet in Figure 10b. The microparticles then flowed toward the mixer mixing them at a pressure of approximately 450 mbar meaning that enhanced mixing occurred through the circulation of liquid at the curved areas and diffusion that facilitated the mixing within the system. It was clear that mixing did therefore occur when inspecting the outlet as illustrated in Figure 10c where we can see a stream of PS beads surrounded by blue dye. The microparticles then progressed toward the concentrator where the stream focused as expected, as seen in Figure 10d.

The final device therefore acted as hypothesized, where the microparticles are separated, mixed, focused and concentrated accordingly. The design however does have its drawbacks, and refinement is necessary as fouling occurs within the microchannels as illustrated in Figure 10b–d which is believed to occur due to the high concentration of particles passing through the device and because of the roughness and dimension variations within the microchannels, allowing for microparticles to settle within the uneven surface. This alongside the other faults described in the previous section shows that even though the components and final device are functional, the design and fabrication of the device may be improved.

The final device separated all the 20 μm PS beads from the 10 and 5 μm beads with an efficiency exceeding 95% since a very minute amount of stray 10 μm beads managed to enter the final stream caused due to the roughness issues previously mentioned. The mixer in the consecutive sections provided full mixing nearly instantaneously allowing for good vicinity of the PS beads and the dye for a duration of more than 85% of the length of the mixer, approximating to two seconds. The concentrator following the mixing procedure concentrated the 20 μm beads by 250% while also further removing some of the 10 μm beads still found in the solution after the initial separation. The full device therefore produced separated 20 μm in a mixed solution with a loss not exceeding 5% to the other outlets due to fabrication errors described earlier. Given that these components show similar results to those of previous authors who utilized CTCs[3,16–20] similar efficiency is expected when repeated with cells of similar sizes.

4. Conclusions and Future Work

In conclusion, through this work, we have managed to design, simulate, and fabricate a variety of passive two-dimensional

microfluidic components and a final design that can effectively manipulate microparticles between 5 and 20 μm in size as needed by flow cytometry applications. The device fabricated can separate PS beads by size ranging between 5 and 20 microns. The device also allows for the enhanced mixing of PS beads, regardless of size and at a variety of flow rates where input pressures between 60 and 1000 mbar were proven successful. These dyed microparticles were concentrated within the device allowing for a 250% reduction from the original volume while also removing microparticles of smaller diameter and focusing the microparticles into distinctive streams based on their size. When compiled, this design has an area footprint of approximately 9 cm^2, as seen in Figure 3, while still acting at very high throughputs at a flow rate of approximately 2 mL min^{-1}. The device also does not require a large sample to function with samples ranging between one to a few milliliters being more than adequate for the robust design to function continuously and efficiently

Acknowledgements

This project has received funding from the European Union's Horizon 2020 research and innovation programme under the Marie Skłodowska-Curie grant agreement No. 945413 and the Universitat Rovira i Virgili (URV). Grant PID2019-108543RB-I00 funded by MCIN/AEI/10.13039/501100011033. The research work presented in this paper is the outcome of a project funded by both institutions under the collaboration framework agreement between the Diputació de Tarragona and the Universitat Rovira i Virgili for the period 2020–2023 with the project code 2021/23: Qualitat de l'aigua. Nous sensors per a la vigilància digital i monitoritzada and the project code 2022/15: "Detecció de microplàstics en aigües del litoral de la província de Tarragona".

Conflict of Interest

The authors declare no conflict of interest.

Data Availability Statement

The data that support the findings of this study are available from the corresponding author upon reasonable request.

Keywords

cell sorting, flow cytometry, labs-on-a-chip, microfluidic devices, microparticle manipulation

Received: March 9, 2023
Revised: May 2, 2023
Published online: May 17, 2023

[1] J. Gong, R. Jaiswal, P. Dalla, F. Luk, M. Bebawy, *Semin. Cell Dev. Biol.* **2015**, *40*, 35.
[2] B. P. Casavant, R. Mosher, J. W. Warrick, L. J. Maccoux, S. M. F. Berry, J. T. Becker, V. Chen, J. M. Lang, D. G. McNeel, D. J. Beebe, *Methods* **2013**, *64*, 137.
[3] H. W. Hou, M. E. Warkiani, B. L. Khoo, Z. R. Li, R. A. Soo, D. S. W. Tan, W. T. Lim, J. Han, A. A. S. Bhagat, C. T. Lim, *Sci. Rep.* **2013**, *3*, 1259.
[4] Y. Liu, S. Wang, H. Xia, X. Tan, S. Song, S. Zhang, D. Meng, Q. Chen, Y. Jin, *J. Transl. Med.* **2022**, *20*, 404.
[5] A. Burklund, A. Tadimety, Y. Nie, N. Hao, J. X. J. Zhang, *Adv. Clin. Chem.* **2020**, *95*, 1.
[6] Y. Gong, N. Fan, X. Yang, B. Peng, H. Jiang, *Electrophoresis* **2019**, *40*, 1212.
[7] A. Kulasinghe, H. Wu, C. Punyadeera, M. E. Warkiani, *Micromachines* **2018**, *9*, 397.
[8] R. Lacroix, S. Robert, P. Poncelet, F. Dignat-George, *Semin. Thromb. Hemostasis* **2010**, *36*, 807.
[9] B. Nasseri, N. Soleimani, N. Rabiee, A. Kalbasi, M. Karimi, M. R. Hamblin, *Biosens. Bioelectron.* **2018**, *117*, 112.
[10] E. K. Sackmann, A. L. Fulton, D. J. Beebe, *Nature* **2014**, *507*, 181.
[11] O. Scheler, W. Postek, P. Garstecki, *Curr. Opin. Biotechnol.* **2019**, *55*, 60.
[12] D. P. Poenar, *Micromachines* **2019**, *10*, 483.
[13] H. Chen, F. Bian, J. Guo, Y. Zhao, *Small Methods* **2022**, *6*, 2200236.
[14] H. Chen, J. Guo, F. Bian, Y. Zhao, *Smart Med.* **2022**, *1*, e20220001.
[15] S. Battat, D. A. Weitz, G. M. Whitesides, *Chem. Rev.* **2022**, *122*, 6921.
[16] E. Pedrol, J. Martínez, M. Aguiló, M. Garcia-Algar, M. Nazarenus, L. Guerrini, E. Garcia-Rico, R. A. Álvarez-Puebla, F. Díaz, J. Massons, *Microfluid. Nanofluid.* **2017**, *21*, 181.
[17] E. Pedrol, M. Garcia-Algar, J. Massons, M. Nazarenus, L. Guerrini, J. Martínez, A. Rodenas, A. Fernandez-Carrascal, M. Aguiló, L. G. Estevez, I. Calvo, A. Olano-Daza, E. Garcia-Rico, F. Díaz, R. A. Alvarez-Puebla, *Sci. Rep.* **2017**, *7*, 3677.
[18] D. Di Carlo, D. Irimia, R. G. Tompkins, M. Toner, *Proc. Natl. Acad. Sci. U.S.A.* **2007**, *104*, 18892.
[19] D. Di Carlo, J. F. Edd, D. Irimia, R. G. Tompkins, M. Toner, *Anal. Chem.* **2008**, *80*, 2204.
[20] L. Zheng, G. Cai, S. Wang, M. Liao, Y. Li, J. Lin, *Biosens. Bioelectron.* **2019**, *124–125*, 143.
[21] S. S. Kuntaegowdanahalli, A. A. S. Bhagat, G. Kumar, I. Papautsky, *Lab Chip* **2009**, *9*, 2973.
[22] A. A. S. Bhagat, S. S. Kuntaegowdanahalli, I. Papautsky, *Lab Chip* **2008**, *8*, 1906.
[23] J. M. Martel, K. C. Smith, M. Dlamini, K. Pletcher, J. Yang, M. Karabacak, D. A. Haber, R. Kapur, M. Toner, *Sci. Rep.* **2015**, *5*, 11300.
[24] E. S. Asmolov, *J. Fluid Mech.* **1999**, *381*, 63.
[25] Y. Morita, T. Itano, M. Sugihara-Seki, *J. Fluid Mech.* **2017**, *813*, 750.
[26] B. Chun, A. J. C. Ladd, *Phys. Fluids* **2006**, *18*, 031704.
[27] A. P. Sudarsan, V. M. Ugaz, *Proc. Natl. Acad. Sci. U.S.A.* **2006**, *103*, 7228.
[28] S. Ookawara, D. Street, K. Ogawa, *Chem. Eng. Sci.* **2006**, *61*, 3714.
[29] T. M. Squires, S. R. Quake, *Rev. Mod. Phys.* **2005**, *77*, 977.
[30] H. A. Stone, A. D. Stroock, A. Ajdari, *Annu. Rev. Fluid Mech.* **2004**, *36*, 381.
[31] A. E. Kamholz, P. Yager, *Sens. Actuators, B* **2002**, *82*, 117.
[32] A. E. Kamholz, B. H. Weigl, B. A. Finlayson, P. Yager, *Anal. Chem.* **1999**, *71*, 5340.
[33] S. H. Wong, M. C. L. Ward, C. W. Wharton, *Sens. Actuators, B* **2004**, *100*, 359.
[34] C. C. Hong, J. W. Choi, C. H. Ahn, *Lab Chip* **2004**, *4*, 109.
[35] A. S. Yang, F. C. Chuang, C. K. Chen, M. H. Lee, S. W. Chen, T. L. Su, Y. C. Yang, *Chem. Eng. J.* **2015**, *263*, 444.
[36] H. Wang, P. Iovenitti, E. Harvey, S. Masood, *Smart Mater. Struct.* **2002**, *11*, 662.
[37] A. Afzal, K. Y. Kim, *J. Mar. Sci. Technol.* **2014**, *22*, 680.

